

CaFe₂As₂: a springboard to investigating Fe-pnictide superconductivity

D. A. Tompsett* and G. G. Lonzarich

Cavendish Laboratory, University of Cambridge, Madingley Road, Cambridge CB3 0HE, UK

(Dated: March 27, 2009)

We present detailed electronic structure calculations for CaFe₂As₂. We investigate in particular the ‘collapsed’ tetragonal and orthorhombic regions of the temperature-pressure phase diagram and find properties that distinguish CaFe₂As₂ from other Fe-pnictide compounds. In contrast to the tetragonal phase of other Fe-pnictides the electronic structure in the ‘collapsed’ tetragonal phase of CaFe₂As₂ is found to be strongly 3D. We discuss the influence of these properties on the formation of superconductivity and in particular we find evidence that both magnetic and lattice interactions may be important to the formation of superconductivity. We also find that the Local Spin Density Approximation is able to accurately predict the ordering moment in the low temperature orthorhombic phase.

PACS numbers: 74.70.Dd, 71.15.Mb, 74.25.Jb

I. INTRODUCTION

The recent discovery of superconductivity in the doped iron pnictide compounds and subsequent improvement in T_c has generated significant interest in uncovering the mechanisms responsible for this novel superconductivity. In the 1,2,2 class of Fe-pnictide compounds including (Ca,Ba,Sr,Eu)Fe₂As₂, superconductivity has been shown under pressure tuning for (Ba,Sr,Eu)Fe₂As₂^{1,2} with transition temperatures as high as 32K. There have been several reports of the presence of superconductivity in the phase diagram of CaFe₂As₂ as it is pressure tuned from the orthorhombic phase into the collapsed tetragonal phase at low temperatures^{3,4}. The determination of the presence of superconductivity has recently been shown to be more complex by measurements made using a Helium pressure medium⁵. It has also been suggested that superconductivity results from the presence of a mixed phase intermediate between the collapsed tetragonal and orthorhombic phases⁶. Therefore, CaFe₂As₂ may be a material that is near the border for the formation of superconductivity and as a result its electronic and magnetic structure have the potential to provide critical information regarding the superconductivity of these compounds.

The Temperature-Pressure phase diagram for CaFe₂As₂ is unusual amongst Fe-pnictide compounds and is shown schematically in Fig. 1. The presence of the ‘collapsed’ tetragonal phase at low temperatures with the application of modest pressures distinguishes this compound from other members of the 1,2,2 family⁷. The low temperature orthorhombic antiferromagnetic phase that occurs at low pressures is common to the 1,2,2 class and is thought to result from the formation of spin density wave (SDW) itinerant magnetism⁸. At high temperatures CaFe₂As₂ exists in a tetragonal structure and is non-magnetic⁹.

In the calculations reported here we seek to consider the electronic structure of CaFe₂As₂ throughout the three key parts of the phase diagram. We investigate the mechanisms for the novel phase transitions and superconductivity of this compound. We also present predictions for future quantum oscillation studies that may experimentally verify the electronic structure.

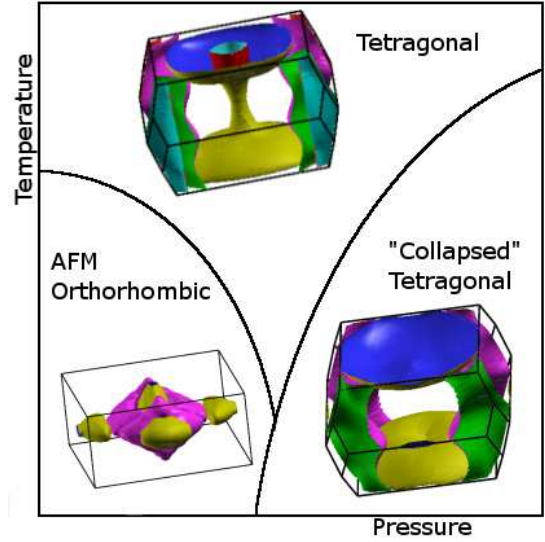


FIG. 1: (Color online) Phase diagram of CaFe₂As₂ showing the Local Spin Density Approximation Fermi surface calculated in this study for each region. The dramatic changes in the Fermi surface as we introduce new order by structural or magnetic phase changes illustrates coupling to the electronic degrees of freedom. This is indicative of the need to consider both magnetic and lattice interactions with the crystal structure when discussing superconductivity in this class of compounds.

II. STRUCTURE AND METHOD

The electronic structures were determined by the Full-Potential LAPW method implemented in WIEN2K¹⁰. In all cases $R_{MT}^{min} K_{max} = 8$ was used. We have used the Local Spin Density Approximation (LSDA) for the correlation functional except where otherwise stated. We

have used the experimental lattice parameters reported for each part of the phase diagram. Further details will be discussed as is relevant to each calculation. Fermi surfaces were visualized with XCrysDen¹¹.

In the following sections we consider each part of the phase diagram in turn. First, we present the results for the ambient pressure tetragonal phase. These results place CaFe_2As_2 in a background from which it may be referenced to other Fe-pnictide systems. We then consider the collapsed tetragonal phase at $P=0.63$ GPa and contrast this electronic structure with the high temperature tetragonal phase. Finally, we consider the antiferromagnetic orthorhombic state and investigate the prediction of the magnetic moment in this phase. With each of these elements of the phase diagram in place, we are then in a position to qualitatively discuss their interplay in determining the magnetic order and possible mechanisms for superconductivity in the system.

III. THE HIGH TEMPERATURE TETRAGONAL PHASE

The crystal structure of the high temperature tetragonal phase of CaFe_2As_2 is in the $I4/mmm$ tetragonal space group with lattice parameters $a = 3.912\text{\AA}$ and $b = 11.667\text{\AA}$ ¹². Calculations of the electronic structure of CaFe_2As_2 in this phase have previously been presented for comparison with X-ray photoelectron spectra¹³. Here, we present details, in particular the form of the Fermi surface, that are important as a point of comparison between CaFe_2As_2 and other Fe-pnictide systems as well as for comparison with CaFe_2As_2 in its collapsed tetragonal structure. We have calculated the electronic structure using $31 \times 31 \times 31$ k-points in the full Brillouin zone and the resulting Fermi surface is shown in Fig. 2(a). During the calculation we relaxed the lattice position of the As atom, z_{As} , from its experimental position of $z_{\text{As}} = 0.3665$ to $z_{\text{As}} = 0.353(0)$ under the LSDA. The Fermi surface obtained is similar to that found in previous calculations for $(\text{Ba},\text{Sr})\text{Fe}_2\text{As}_2$ ^{8,14}.

It is intriguing to note the similarity between this Fermi surface and that of MgB_2 which also possesses two concentric warped cylinders at the zone corners as well as a flat 3D pocket in a similar position to the flared section of the dumbbell surface. The primary difference is the lack of a further 3D pocket about Γ which occurs in MgB_2 , but not in CaFe_2As_2 . In MgB_2 it is the two outer cylinders which couple to the lattice to form superconductivity¹⁵.

IV. THE ‘COLLAPSED’ TETRAGONAL PHASE

In the collapsed tetragonal phase the crystal maintains the $I4/mmm$ symmetry of the high temperature tetragonal phase, but undergoes a dramatic reduction in the c-axis lattice parameter of approximately 6% while simultaneously the in-plane dimension increases

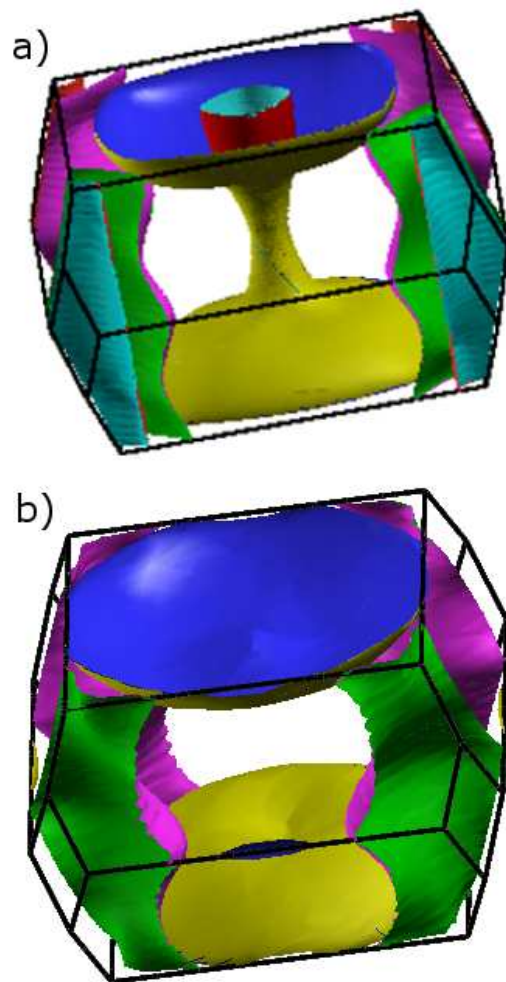


FIG. 2: (Color online) a) The Fermi surface of CaFe_2As_2 in the high temperature tetragonal phase. b) The Fermi surface of CaFe_2As_2 in the ‘collapsed’ tetragonal phase at $P=0.63$ GPa⁹. In contrast to the Fermi surface in the ambient pressure tetragonal phase we find just two Fermi surface sheets. One strongly 3D hole sheet that we refer to as the pillow as well as a strongly corrugated electron cylinder at the zone corners. The 3D nature of the hole sheet makes the possibility of SDW instabilities due to nesting in the Fermi surface less clear.

by approximately 2%. The unit cell is effectively squashed. At $P=0.63$ GPa the lattice parameters are $a = 3.9780(1)\text{\AA}$ and $b = 10.6073(7)\text{\AA}$ ⁹. We have calculated the electronic structure for this phase using a $39 \times 39 \times 39$ k-point grid. The resulting Fermi surface is shown in Fig. 2(b). In Table I we also present the quantum oscillation frequencies and associated band masses for \mathbf{B} parallel to c-axis. Experimental comparison with these values has the ability to verify the electronic structure obtained in our calculations and the experimental mass enhancement can indicate the strength of correlations in the system.

A critical observation of this investigation is the dra-

TABLE I: Theoretical quantum oscillation frequencies and band masses for the collapsed tetragonal phase with the magnetic field, \mathbf{B} , parallel to the c-axis.

Orbit ^a	Frequency (kT)	Band Mass (m_e)
α_1	3.64	1.25
α_2	6.02	2.17
α_3	7.19	2.15
β	16.0	2.40

^a α denotes the warped cylinder around the zone corner in Fig. 2(b), β is the large pillow surface.

matic difference between the Fermi surfaces of the collapsed tetragonal phase and the high temperature tetragonal phase. The difference involves two key alterations. Firstly, in the collapsed phase we find a Fermi surface that is composed of just two sheets. Secondly, due to the further reduction in the c-axis lattice parameter the hole pocket is now very 3D. Therefore, the electronic structure of this collapsed tetragonal phase is distinct from both the high temperature tetragonal phase and that of other members of the Fe-pnictide family.

It has been suggested that magnetically mediated Cooper pairing is more robust in 2D systems¹⁶ and therefore the 3D Fermi surface of the collapsed tetragonal phase may give rise to lower superconducting transition temperatures than similar 2D systems. In fact if we consider the pressure induced superconducting transitions of the (Ba,Sr,Eu)Fe₂As₂ family then we find support for this idea. (Ba,Sr,Eu)Fe₂As₂ show maximal pressure induced transition temperatures of approximately 32K, 28K and 29K respectively^{1,2}. Each of these compounds shows a more 2D paramagnetic electronic structure around the superconducting transition than we have found here for CaFe₂As₂. Therefore, the explanation for the lower transition temperature of 12K^{3,4}, or absence of superconductivity as reported by Lee *et al.*⁶, may rely on the different dimensionality of the Fermi surface in this collapsed tetragonal region.

The dramatic change in Fermi surface topology in moving through the transition from the high temperature to the collapsed tetragonal phase is produced by a reduction in lattice volume of just 5%. This is indicative of a significant coupling between the electronic and lattice degrees of freedom. A phononic influence in combination with magnetic interactions may therefore be active in producing superconductivity in these compounds as has been suggested for BaNi₂As₂¹⁷.

V. THE ORTHORHOMBIC PHASE

In the low temperature and pressure region of its phase diagram CaFe₂As₂ is antiferromagnetic (AFM) in the $Fmmm$ orthorhombic structure. The lattice parameters are $a=5.506(2)\text{\AA}$, $b=5.450(2)\text{\AA}$, and $c=11.664(6)\text{\AA}$ and $z_{As} = 0.36642(5)$ ¹⁸. The magnetic

moment is $0.80(5)\mu_B/\text{Fe}$ ¹⁸. The conventional magnetic unit cell is the same as that of the crystal structure, but the symmetry is reduced due to the magnetic order.

We have evaluated the electronic and magnetic structure for the experimentally determined magnetic order¹⁸ using both the Generalized Gradient Approximation of Perdew-Burke-Ernzerhof (GGA) and the LSDA correlation functionals. For all calculations in this antiferromagnetic phase we have used $23 \times 23 \times 10$ k-points in the Brillouin zone.

First, we applied the GGA to the AFM structure. Relaxing the As position within the AFM calculation results in, $z_{As} = 0.3659$, which matches the experimental value closely, but the predicted moment of $1.84\mu_B/\text{Fe}$ overestimates the experimental value by a factor of more than 2. Overestimates of this scale for the magnetic moment in Fe-pnictides while applying the GGA have been widely reported¹⁹.

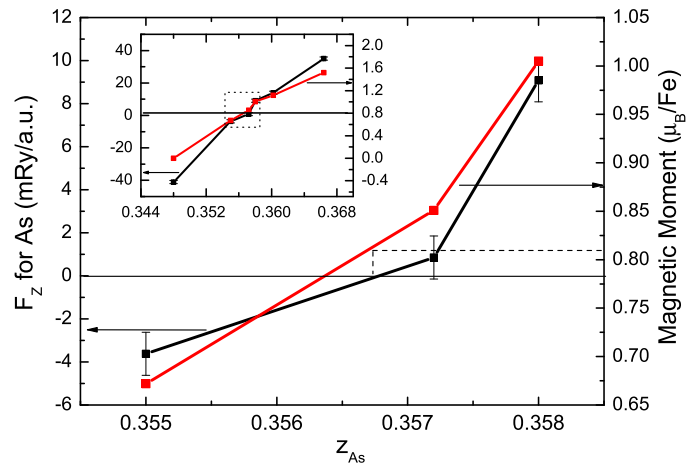


FIG. 3: (Color online) Plot of the force on the As atom (black) and the magnetic moment of Fe (red) versus the lattice parameter z_{As} in CaFe₂As₂. The forces and magnetic moments were determined under the Local Spin Density Approximation. The main figure shows the region about $F_z = 0$ where the As position is relaxed into its equilibrium structure. The inset is a view of this plot over a wider scale of z_{As} . The solid horizontal line indicates where the force $F_z = 0$. The dashed lines in the main figure are to illustrate the value of the moment in μ_B/Fe that occurs when $F_z = 0$.

Secondly, we applied the LSDA to the antiferromagnetic structure while relaxing the value z_{As} . We find that the relaxation of the As coordinate is significant, from $z_{As} = 0.3664$ experimentally to $z_{As} = 0.3567$. In Fig. 3 we have plotted both the force on the As atom, F_z , and the magnetic moment of Fe as a function of its relaxation to the plane of the Fe atoms. Very importantly, this figure shows that the moment approaches $0.81 \pm 0.02\mu_B/\text{Fe}$ as F_z tends towards zero i.e. when the As is in its crystallographic equilibrium position. This is in close agreement with the experimental reported moment of $0.80(5)\mu_B/\text{Fe}$ ¹⁸. To confirm this result we have applied the same method to SrFe₂As₂ and BaFe₂As₂.

TABLE II: Comparison between the magnetic moment of 1,2,2 compounds predicted by the LSDA when the As position is relaxed in the antiferromagnetic phase and the experimental values^{18,20,21,22}.

Compound	LSDA		Experimental	
	μ (μ_B)/ Fe^a	z_{As}	μ (μ_B)/ Fe	z_{As}
CaFe ₂ As ₂	0.81±0.02	0.3567	0.80(5)	0.36642(5)
SrFe ₂ As ₂	0.97±0.03	0.3507	0.94(4) ^b	0.3612(3)
BaFe ₂ As ₂	0.86±0.02	0.3444	0.87(3)	0.35406(7)

^aThe errors given are calculated from the convergence of the force on the As atom.

^bMore recent measurements²³ have found $\mu = 1.01\mu_B/Fe$.

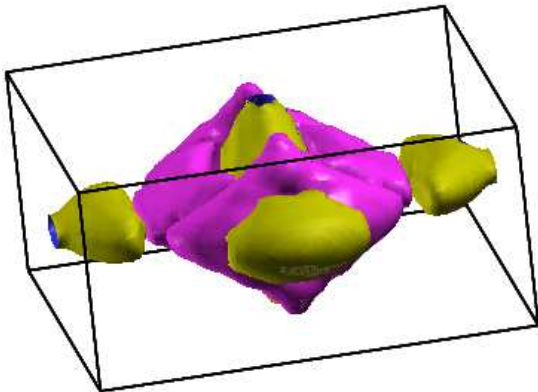


FIG. 4: (Color online) The Fermi surface of CaFe₂As₂ calculated using the Local Spin Density Approximation with the As coordinate relaxed in the antiferromagnetic phase.

The results are summarized in Table II and give strong agreement with experiment.

It has been suggested that overestimations of the moment by Density Functional Theory may indicate quantum spin fluctuations. Such effects are not fully accounted for under Density Functional Theory which is mean-field in nature. Our study, however, suggests that a relaxation of the internal coordinates to the LSDA equilibrium position for As in the AFM phase is sufficient to permit the accurate prediction of the magnetic

moment. In some previous work the As coordinate has been relaxed in a non-magnetic calculation^{9,24} which has resulted in overestimates of the moment of approximately $1.5\mu_B/Fe$. Other work has shown the presence of a smaller moment under the LSDA in LaFeAsO²⁵ and BaFe₂As₂¹⁴, but with less accurate correspondence with experiment than is shown in this study. Together, these findings suggest that the preceding overestimation of the moment should not be used as evidence for zero-point fluctuations in this strongly antiferromagnetic material.

The Fermi surface of CaFe₂As₂ for the LSDA calculation is shown in Fig. 4. Most of the Fermi surface is gapped away by the additional ordering vector to leave the small pockets shown. Analysis of the associated quantum oscillation frequencies shows broad agreement with the recent experimental results of Harrison *et al.*²⁶

The results presented here have the potential to motivate further studies of the magnetic structure in these compounds that are both qualitatively and quantitatively accurate.

VI. SUMMARY AND CONCLUSIONS

The phase diagram of Fig. 1 illustrates that the CaFe₂As₂ Fermi surface changes dramatically through magnetic and structural phase transitions. This is suggestive that both magnetic and lattice interactions should be considered in the formulation of any model of superconductivity in this compound.

The greater three dimensionality of the collapsed phase Fermi surface suggest that pairing due to magnetic interactions may be weaker and this may explain the lower superconducting T_c ^{3,4}, or absence of superconductivity⁵, in CaFe₂As₂ when compared to (Ba,Sr,Eu)Fe₂As₂ under pressure.

Predictions for quantum oscillation experiments on the collapsed tetragonal phase have been given. We have also demonstrated that the magnetic moment in the AFM orthorhombic phase may be accurately calculated under the LSDA if the As coordinate is relaxed within an AFM calculation.

* Electronic address: dat36@cam.ac.uk

¹ P. L. Alireza, Y. T. C. Ko, J. Gillett, C. M. Petrone, J. M. Cole, G. G. Lonzarich, and S. E. Sebastian, J. Phys. Condens. Mat. **21**, 012208 (2009).

² C. F. Miclea, M. Nicklas, H. S. Jeevan, D. Kasinathan, Z. Hossain, H. Rosner, P. Gegenwart, C. Geibel, and F. Steglich, arXiv:0808.2026 (unpublished).

³ M. S. Torikachvili, S. L. Bud'ko, N. Ni, and P. C. Canfield, Phys. Rev. Lett. **101**, 057006 (2008).

⁴ T. Park, E. Park, H. Lee, T. Klimczuk, E. D. Bauer, F. Ronning, and J. D. Thompson, J. Phys. Condens. Mat. **20**, 322204 (2008).

⁵ W. Yu, A. A. Aczel, T. J. Williams, S. L. Bud'ko, N. Ni,

P. C. Canfield, and G. M. Luke, Phys. Rev. B **79**, 020511 (2009).

⁶ H. Lee, E. Park, T. Park, F. Ronning, E. D. Bauer, and J. D. Thompson, arXiv:0809.3550 (unpublished).

⁷ R. J. McQueeney, S. O. Diallo, V. P. Antropov, G. D. Samolyuk, C. Broholm, N. Ni, S. Nandi, M. Yethiraj, J. L. Zarestky, J. J. Pulikotil, et al., Phys. Rev. Lett. **101**, 227205 (2008).

⁸ S. E. Sebastian, J. Gillett, N. Harrison, P. H. C. Lau, D. J. Singh, C. H. Mielke, and G. G. Lonzarich, J. Phys. Condens. Mat. **20**, 422203 (2008).

⁹ A. Kreyssig, M. A. Green, Y. Lee, G. D. Samolyuk, P. Zajdel, J. W. Lynn, S. L. Bud'ko, M. S. Torikachvili, N. Ni,

- S. Nandi, et al., Phys. Rev. B **78**, 184517 (2008).
- ¹⁰ K. Schwarz and P. Blaha, Comput. Mater. Sci. **28**, 259 (2003).
 - ¹¹ A. Kokalj, Comp. Mater. Sci. **28**, 155 (2003).
 - ¹² N. Ni, S. Nandi, A. Kreyssig, A. I. Goldman, E. D. Mun, S. L. Bud'ko, and P. C. Canfield, Phys. Rev. B **78**, 014523 (2008).
 - ¹³ E. Kurmaev, J. McLeod, A. Buling, N. Skorikov, A. Moewes, M. Neumann, M. Korotin, Y. Izyumov, N. Ni, and P. Canfield, arXiv:0902.1141 (unpublished).
 - ¹⁴ D. J. Singh, Phys. Rev. B **78**, 094511 (2008).
 - ¹⁵ I. Mazin and V. Antropov, Physica C **385**, 49 (2003).
 - ¹⁶ P. Monthoux and G. Lonzarich, Phys. Rev. B **63**, 054529 (2001).
 - ¹⁷ A. Subedi and D. J. Singh, Phys. Rev. B **78**, 132511 (2008).
 - ¹⁸ A. I. Goldman, D. N. Argyriou, B. Ouladdiaf, T. Chatterji, A. Kreyssig, S. Nandi, N. Ni, S. L. Bud'ko, P. C. Canfield, and R. J. McQueeney, Phys. Rev. B **78**, 100506 (2008).
 - ¹⁹ D. Singh, arXiv:0901.2149 (unpublished).
 - ²⁰ J. Zhao, W. Ratcliff, II, J. W. Lynn, G. F. Chen, J. L. Luo, N. L. Wang, J. Hu, and P. Dai, Phys. Rev. B **78**, 140504 (2008).
 - ²¹ M. Tegel, M. Rotter, V. Weiss, F. M. Schappacher, R. Pottgen, and D. Johrendt, J. Phys. Condens. Mat. **20**, 452201 (2008).
 - ²² Q. Huang, Y. Qiu, W. Bao, M. A. Green, J. W. Lynn, Y. C. Gasparovic, T. Wu, G. Wu, and X. H. Chen, Phys. Rev. Lett. **101**, 257003 (2008).
 - ²³ K. Kaneko, A. Hoser, N. Caroca-Canales, A. Jesche, C. Krellner, O. Stockert, and C. Geibel, Phys. Rev. B **78**, 212502 (2008).
 - ²⁴ I. I. Mazin, M. D. Johannes, L. Boeri, K. Koepernik, and D. J. Singh, Phys. Rev. B **78**, 085104 (2008).
 - ²⁵ T. Yildirim, Phys. Rev. Lett. **101**, 057010 (2008).
 - ²⁶ N. Harrison, R. D. McDonald, C. H. Mielke, E. D. Bauer, F. Ronning, and J. D. Thompson, arXiv:0902.1481 (unpublished).